The Seasonal Footprinting Mechanism in the Pacific: Implications for ENSO*

DANIEL J. VIMONT, JOHN M. WALLACE, AND DAVID S. BATTISTI

Department of Atmospheric Sciences, University of Washington, Seattle, Washington

(Manuscript received 15 February 2002, in final form 23 July 2002)

ABSTRACT

Midlatitude atmospheric variability is identified as a particularly effective component of the stochastic forcing of ENSO. This forcing is realized via a seasonal footprinting mechanism (SFM), in which the tropical atmosphere is forced during the spring and summer by SST anomalies generated by midlatitude atmospheric variability during the previous winter. The strong relationship between the SFM and ENSO may serve to enhance ENSO predictability and supports the view that ENSO is linearly stable in nature.

1. Introduction and motivation

In a companion study, Vimont et al. (2003)[1] (see also Vimont et al. 2002) identify a mechanism by which midlatitude atmospheric variability can impact tropical ENSO-like variability in the Commonwealth Scientific and Industrial Research Organisation (CSIRO) coupled general circulation model (CGCM), and label the mechanism the *seasonal footprinting mechanism* (SFM). The SFM may be summarized as follows. During the winter season, intrinsic atmospheric variability in the midlatitudes [with a spatial structure that closely resembles the observed so-called North Pacific oscillation (NPO) of Walker and Bliss (1932) and Rogers (1981)] imparts an SST ''footprint'' onto the ocean via changes in the net surface heat flux. This SST footprint persists into the late spring and summer seasons. The subtropical (0°–20°N) portion of the SST footprint, in turn, forces a pattern of atmospheric circulation anomalies that includes zonal wind stress anomalies along the equator. Finally, the coupled tropical atmosphere–ocean system responds to the summer zonal wind stress anomalies (produced through the SFM) through coupled dynamics, producing an equatorially symmetric, ENSO-like pattern of variability. In the CSIRO CGCM, the SFM accounts for nearly 40% of the interannual variability, and up to 70% of the interdecadal variability along the equator (Vimont et al. 2003). Vimont et al. (2003) note that the SFM is not the primary ENSO mechanism but rather is a means of characterizing the stochastic forcing essential to the CSIRO CGCM's linearly stable ENSO mode (Vimont et al. 2002). We note that similar behavior is found in the numerical simulations of Barnett et al. (1999) and Pierce et al. (2000). A similar influence of remote (or midlatitude) variability on the Tropics has been identified in observational studies of the Atlantic (Chiang et al. 2001, manuscript submitted to *J. Climate*; Czaja et al. 2002).

The importance of the SFM in contributing to interannual and interdecadal equatorial variability in the CSIRO CGCM begs the question, is the SFM operative in nature? A comparison of composite maps of winter (November–March, hereafter NDJFM) averaged SST during ENSO years with the sea level pressure (SLP) anomalies 1 yr earlier in Fig. 1 suggests that it is. A statistically significant NPO-like pattern is indeed observed to precede ENSO by 1 yr.

Motivated by the lag relationship in Fig. 1 and the importance of the SFM in the CSIRO CGCM, this study aims to further investigate the behavior of the SFM in the observational record. Data and methodology are described in section 2. Section 3 presents a statistical analysis of the SFM followed by an investigation of the physical processes behind SFM. Finally, section 4 presents a discussion of the results.

2. Data and methods

The seasonal connections outlined in the description of the SFM in section 1 provide a natural framework for the definition of the SFM in the observed record. We apply maximum covariance analysis (MCA; also

* Joint Institute for the Study of the Atmosphere and Ocean Contribution Number 901.

[1] Due to the strong similarities between the current results and methods, and the results presented in a heirarchy of CGCMs by Vimont et al. (2003), the reader may wish to refer to that manuscript.

Corresponding author address: Dr. Daniel J. Vimont, Dept. of Atmospheric Sciences, University of Washington, JISAO, Box 354235, Seattle, WA 98195-4235.
E-mail: dvimont@atmos.washington.edu

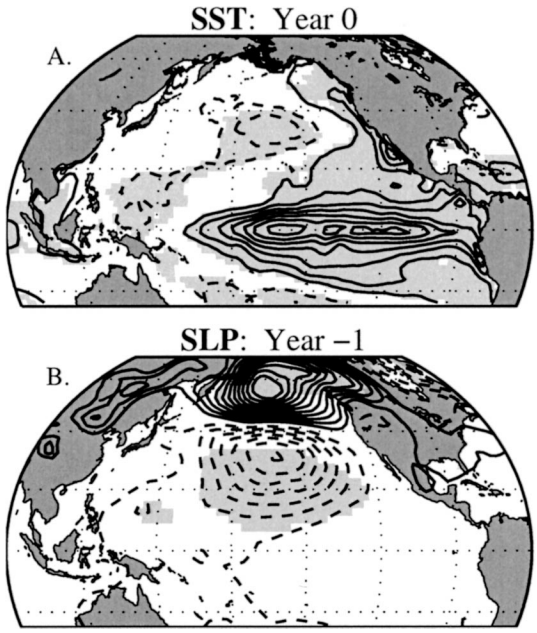

FIG. 1. Composites around the winter mean (NDJFMA) CTI (the CTI is defined as SST averaged from 6°S–6°N, 180°–90°W and is a commonly used index to describe ENSO variability; Mitchell and Wallace 2001, manuscript submitted to *J. Climate*): (a) Simultaneous SST (NDJFM-averaged), contour interval 0.15°C; (b) SLP (NDJFM-averaged) 1 yr earlier than the SST map, contour interval 0.2 hPa. The SST map is defined as one-half the difference between SST averaged over years where the winter CTI exceeds one std dev, and SST averaged over years where the winter CTI is less than minus one std dev. The SLP map is constructed in a similar fashion, except around the years 1 yr prior to those used for the SST map. Positive contours are solid, negative contours are dashed, and the zero contour has been omitted. Regions where the *t* score (based on a difference in means) exceeds the 95% confidence level are lightly shaded. For reference, the semiannually resolved CTI is plotted in Fig. 6a.

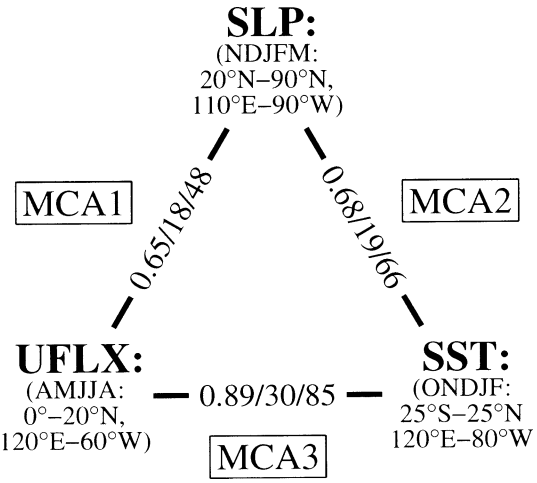

FIG. 2. Graphic illustration of the data, statistical method, and summary statistics used in this analysis. The summary statistics are in the following format: *r* / NC / SCF, where *r* is the correlation between the two resulting time series, NC is the normalized covariance between the two datasets, and SCF is the squared covariance fraction explained by the leading statistical mode.

referred to as singular value decomposition analysis; Bretherton et al. 1992) to the three pairs of variables essential to the SFM: winter midlatitude SLP, summer Northern Hemisphere tropical zonal wind stress, and winter (11 months later than the SLP data) tropical SST. MCA is used on the three pairs of fields with the hopes that three separate results will provide stronger evidence than the results of MCA applied to any single pair of fields. The three MCAs and the data domains are summarized in Fig. 2.

Data used for the MCA are taken from the National Centers for Environmental Prediction–National Center for Atmospheric Research (NCEP–NCAR) 40-yr Reanalysis Project (Kalnay et al. 1996), including SST [Reynolds reanalysis from 1982 onward, and Met Office (UKMO) Global Sea Ice and Sea Surface Temperature (GISST) before 1982]. The domains over which the data are retained, as well as the time intervals over which data are averaged, are displayed in Fig. 2. For the remainder of this study, the terms ''winter (0),'' ''summer (0),'' and ''winter (+1)'' will refer to the consecutive seasons over which SLP (NDJFM), zonal wind stress (April–August, hereafter AMJJA), and SST (October–February, hereafter ONDJF) are averaged, respectively. Prior to performing MCA, the 53-yr records (1949–2001) were spatially smoothed[2] for computational efficiency, and detrended. Next, the winter (0) cold tongue index (CTI) was linearly removed from the data,[3] and the data were standardized. The removal of the winter (0) CTI ensures that the summer (0) zonal wind stress and winter (+1) SST are independent of ENSO variability that may have occurred during the *preceding* winter. While the removal of the winter (0) CTI is not necessary to obtain the results presented herein, it serves to ensure that the seasonal relationships identified by the MCA are dominated by the SFM and not merely by the seasonality of ENSO.

In section 3, outgoing longwave radiation (OLR) is used as a proxy for tropical precipitation anomalies. Interpolated OLR data [described in Liebmann and Smith (1996)] are defined from 1979 to 2001. [All data are from the National Oceanic and Atmospheric Administration–Cooperative Institute for Research in Environmental Sciences (NOAA–CIRES) Climate Diagnostics Center Web site at http://www.cdc.noaa.gov/.]

Unless stated otherwise, statistical significance is inferred when correlations (or composite differences) exceed the 95% confidence interval, based on a two-tailed Student's *t* test. For the correlations, the number of degrees of freedom is determined via the method outlined in Bretherton et al. (1999).

[2] Each set of four adjoining grid points (two latitudinal points by two longitudinal points) was averaged together.

[3] That is, the winter (0) CTI is removed from the contemporaneous SLP, the following summer (0) zonal wind stress (lag +½ yr) and the following winter (+1) SST (lag +1 yr).

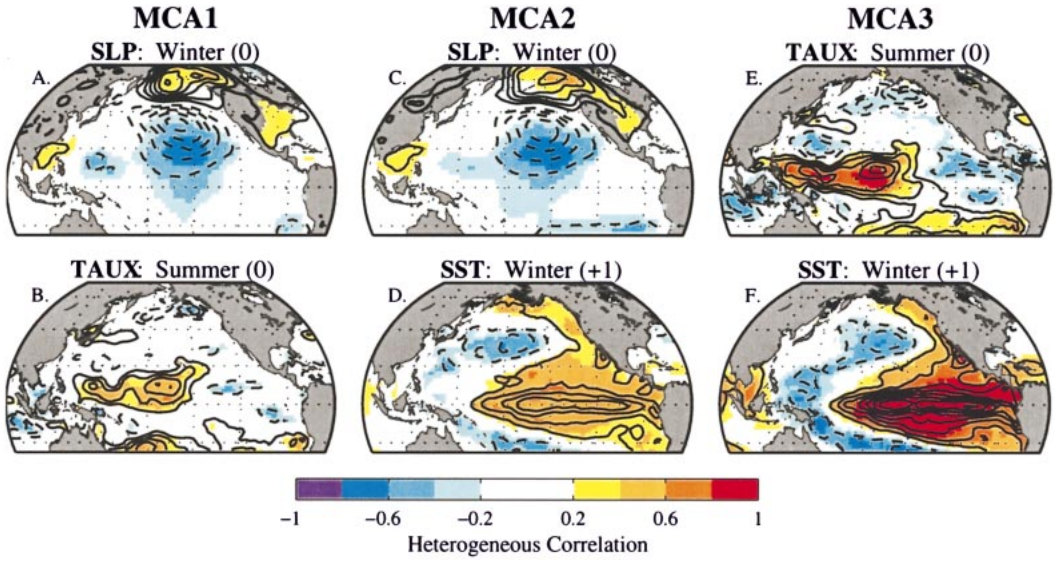

FIG. 3. Leading heterogeneous patterns for the three separate MCA sets described in Fig. 2: (a), (b) SLP and zonal wind stress, respectively, from MCA1; (c), (d) SLP and SST from MCA2; (e), (f) zonal wind stress and SST from MCA3. Units are 0.20 hPa (std dev)$^{-1}$ for SLP; 0.02 dyn cm^{-2} (std dev)$^{-1}$ for zonal wind stress; 0.15°C (std dev)$^{-1}$ for SST. Positive contours are solid, negative contours are dashed, and the zero line has been omitted. The correlation coefficient is shaded and is displayed only where it exceeds the 95% confidence level, based on a two-tailed Student's *t* test.

3. Results

a. MCA results

The statistical results from the MCA are summarized in Fig. 2. The summary statistics in Fig. 2 indicate that the fields included in the analysis are strongly coupled. The leading pairs of heterogeneous regression maps resulting from the MCA are presented in Fig. 3.[4] Each of the maps is presented with dimensional units, indicating the typical amplitude of anomalies associated with the respective MCA mode. The correlation is shaded and is only displayed where it is statistically significant at the 95% confidence level.

Figures 3a,b show the leading pair of coupled patterns for MCA1 [winter (0) midlatitude SLP and summer (+1) Northern Hemisphere tropical zonal wind stress]. The SLP pattern in Fig. 3a bears a strong resemblance to the SLP map in Fig. 1, showing a dipole SLP pattern with centers of action on either side of about 45°N. The light shading in the SLP map highlights the importance of the southern lobe of this dipole, indicative of weakened trades throughout the subtropics. Vimont et al. (2003) find that these reduced trades are essential for forcing the subtropical portion of the SST footprint in the CSIRO CGCM, via reduction of upward latent heat flux, and reduced frictional convergence (and hence reduced cloudiness and an increase in downward solar radiation) in the Tropics. We note that an analysis of intraseasonal (and hence temporally independent of interannual ENSO) NPO variability in the observed record (Vimont 2002, not shown) reproduces these characteristics. During the following summer, the tropical zonal wind stress in Fig. 3b is dominated by positive anomalies in the western and central tropical Pacific, extending from the equator to about 15°–20°N. Similar zonal wind stress anomalies are found in the composites during the onset stage of El Niño and La Niña events, by Harrison and Larkin (1998) and Larkin and Harrison (2001), respectively. The pair of patterns in Figs. 3a,b bears a strong resemblance to the results from the CSIRO CGCMs (Vimont et al. 2001, 2003).

Results from MCA2 [winter (0) midlatitude SLP and winter (+1) tropical SST], plotted in Figs. 3c,d, closely resemble the the composite maps in Fig. 1. Like the results from MCA1, the SLP map in Fig. 3c bears a strong resemblance to the NPO and underscores the importance of weakened trades throughout the subtropics, which are an integral part of that pattern.

The strongly coupled regression maps for MCA3 [summer (0) tropical zonal wind stress and winter (+1) tropical SST], shown in Figs. 3e,f, are dominated by the development and mature stage of ENSO (cf. Harrison and Larkin 1998). The strong correspondence between the zonal wind stress time series from MCA3 and MCA1 ($r = 0.94$) indicate that much of the pattern seen in Fig. 3e is a consequence of previous winter's NPO-like SLP anomalies. Like the zonal wind stress map from MCA1 (Fig. 3b), the tropical zonal wind stress is dominated by weakened trades in the western and central equatorial Pacific, from the equator to 15°–20°N.

[4] The MCAs were calculated using the domains noted in Fig. 2. The maps in Fig. 3 are generated by regressing the respective heterogeneous field onto the time series from each MCA result.

b. Physical consistency

The results from section 3a statistically establish the seasonal relationships outlined by Vimont et al. (2003). In this section, we present evidence that these seasonal relationships are physically consistent. For the remainder of this section, we will use the SLP time series from MCA2 (hereafter referred to as WIN_NPO) to represent the NPO during winter (0).

In accord with the SFM, we except the winter NPO-like SLP anomalies to generate SST anomalies that persist into the summer season, and force equatorial zonal wind stress anomalies (as in Fig. 3). The first element of this causal chain is demonstrated by the regression maps of summer (0) SST and winter (0) net surface heat flux onto WIN_NPO, shown in Fig. 4a.[5] To highlight the SST anomalies that are associated with the SFM (as opposed to those associated with the developing ENSO event), the summer (0) CTI has been removed from the summer (0) SST field. The summer (0) SST map bears a strong resemblance to the patterns found by Deser and Timlin (1997, their Fig. 9) to be caused by the west Pacific teleconnection pattern,[6] and to the SST footprint found by Vimont et al. (2003) in the CSIRO CGCMs. We note that removal of the summer (0) CTI (presumably forced by the SFM) reduces the amplitude of the summer (0) off-equatorial SST anomalies by 25%–50%. Figure 4a indicates that over most of the Tropics and subtropics, positive SST anomalies during summer (0) are collocated with downward net surface heat flux during the previous winter (0). One exception is found in the western equatorial Pacific, which will be commented on later. Given realistic mixed-layer depths, the magnitude of the fluxes in Fig. 4a is consistent with the magnitude of SST anomalies in April, within about 50% (not shown). The relationship in Fig. 4a confirms that winter (0) NPO-like variability forces the SST footprint, and that the SST footprint persists into the summer season.

Analysis of the individual heat flux components indicates that the net heat flux in Fig. 4b is dominated by the surface latent heat flux over most of the Pacific. The latent heat flux may, in turn, be separated (via a standard bulk formula) into contributions from changes in surface wind speed, and changes in the sea–air specific humidity gradient. Not surprisingly, maps of these two components indicate a close compensation between warming due to reduced surface wind speed, and cooling due to an increased specific humidity gradient, with the wind-induced warming dominating. We interpret this compensation as being due to the following mechanism. As the winds weaken in response to the NPO-like SLP anomalies, the oceanic mixed layer warms, increasing the saturated specific humidity at the sea surface. This increase in the sea air specific humidity gradient partially counteracts the warming by the reduced wind speed. We note that the structure of the latent heat flux components, and the compensation, are also evident in the Comprehensive Ocean–Atmosphere Data Set (COADS), though the structure and sign of latent heat flux anomalies in the western equatorial Pacific differ from those in the NCEP reanalysis, implying that the net heat flux may not be trusted there.

Through the SFM, the summer (0) zonal wind stress anomalies are forced by the underlying SST footprint, which should also be evidenced by changes in the strength and location of the summer ITCZ. The atmospheric response to the SST footprint is demonstrated in the regression maps of summer (0) OLR (OLR anom-

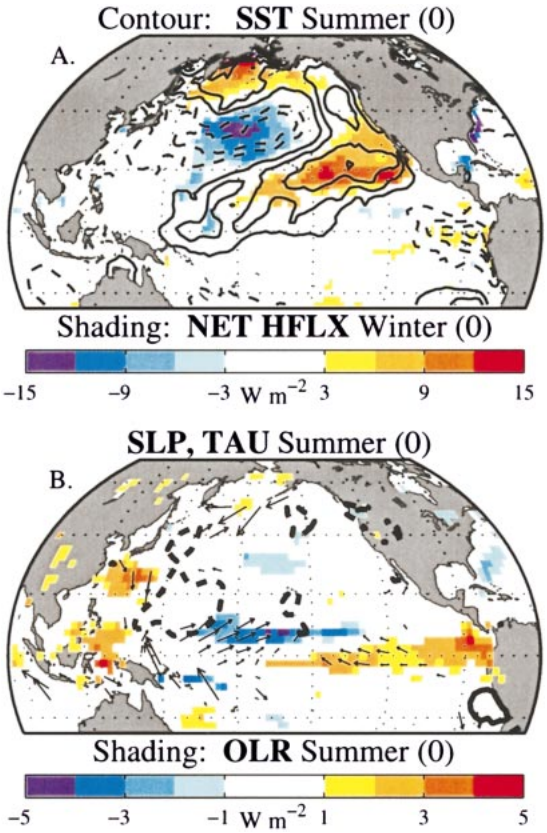

FIG. 4. (a) Regression maps of summer (0) SST (with summer CTI linearly removed) [contours; contour interval 0.075°C (std dev)$^{-1}$] shown together with the winter (0) net surface heat flux (shading). Both fields are regressed onto the winter (0) WIN_NPO index. The net heat flux is shown only where the correlation is significant at the 95% confidence level. (b) Summer (0) OLR (shading), and wind stress (vectors) regressed onto the winter (0) WIN_NPO index. Also contoured is the ±0.4 correlation between summer (0) SLP and WIN_NPO. OLR and wind stress are shown only where OLR and surface wind speed are significantly correlated with WIN_NPO at the 90% and 80% confidence levels, respectively. An SLP correlation of 0.4 is significant at the 90% level over most of the domain. All maps in (b) are generated using the 1979–2001 record.

[5] Maps generated by regression onto the SLP time series from MCA1 are nearly identical.

[6] WIN_NPO is highly correlated with the time series for the west Pacific, and east Pacific teleconnection patterns, as defined by NCEP (see http://www.cpc.ncep.noaa.gov/data/teledoc/telecontents.html).

alies covary negatively with precipitation) and wind stress onto WIN_NPO, shown in Fig. 4b. Also shown in Fig. 4b is the summer (0) SLP correlation onto the same index. All maps are generated by regressing (or correlating) data from 1979 to 2001 (the time period of record of the OLR data) onto the previous winter (0) WIN_NPO index for the same years. As with the summer SST anomalies in Fig. 4a, the summer (0) CTI has been removed from the data prior to generating the regression and correlation maps.

The OLR map in Fig. 4b indicates an intensification and slight northward shift in the summer ITCZ, presumably caused by the positive SST anomalies in the northern subtropics, and the northward anomalous tropical SST gradient seen in Fig. 4a. The OLR anomalies are significant over much of the Tropics and are duplicated in similar regression maps of Climate Prediction Center Merged Analysis of Precipitation (CMAP) precipitation (not shown). The intensification and northward shift of the ITCZ is consistent with westerly wind stress anomalies in the western equatorial Pacific (also seen in Figs. 3b,e) and cyclonic SLP anomalies north and northwest of the precipitation anomalies [this circulation bears a strong resemblance to the atmospheric response to asymmetric heating, as simulated in Gill (1980)]. Atmospheric GCM simulations forced by a similar subtropical SST footprint produce very similar results (see Fig. 9 of Vimont et al. 2003). A detailed analysis of the roles of elevated heating and surface temperature gradients in producing the circulation anomalies in Fig. 4b (as in Chiang et al. 2001) is beyond the scope of this study. We note that if the summer (0) CTI is *not* removed prior to the regressions, westerly wind stress anomalies extend across the basin, due to the onset of ENSO. The easterly wind stress anomalies in Fig. 4b may arise due to nonlinearities in the eastern Pacific response to positive and negative phases of ENSO during summer (0), or to the inability of the 23-yr dataset (used in Fig. 4b) to fully represent ENSO and the SFM.

The last link in the connection between the NPO-like SLP anomalies and ENSO involves the eventual development of ENSO in response to the wind stress anomalies produced through the SFM. This response is inferred through the temporal evolution of variability associated with the SFM, shown in Fig. 5. Indices that represent 1) the NPO, 2) the subtropical portion of the NPO-forced SST footprint, 3) the equatorial Kelvin wave forcing function K_f (explained shortly), and 4) the CTI are generated by the method described in the appendix. Each index indicates the relative strength of variability at a given monthly lag from the winter (0) WIN_NPO index. For example, the NPO evolution (thick solid line in Fig. 5) indicates that the NPO is strongest during January of winter (0), when WIN_NPO is defined. The SST footprint index (thick dashed line) is interpreted similarly. The K_f index (thin solid line with circles) indicates the effectiveness of wind stress

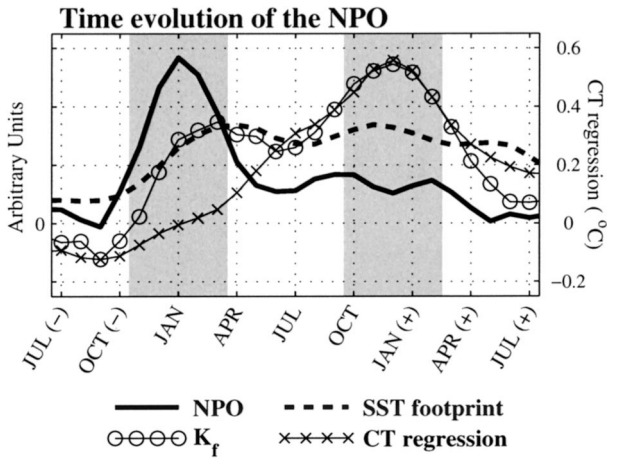

FIG. 5. Temporal evolution of variability associated with the SFM. Each index indicates the relative strength of variability at a given lag from WIN_NPO. The method of calculation for each curve is presented in the appendix.

anomalies [at a given lag from the winter (0) WIN_NPO index] in the western and central Pacific (120°E–150°W) at forcing oceanic equatorial Kelvin waves. The K_f index is scaled such that positive values indicate forcing of downwelling Kelvin signals, which will tend to warm the eastern equatorial Pacific. Finally, the CTI evolution (thin solid line with ×'s) is expressed by the lagged regression coefficient between the CTI (for a given month) and WIN_NPO. Each curve in Fig. 5 is generated using the entire record. We note that the relationships in Fig. 5 are strongest in the latter part of the record (1979–2001), an observation that is confirmed by investigating similar relationships in COADS.

The winter (0), summer (0), and winter (+1) time periods may be roughly characterized by the development of the SST footprint, the transition phase (from SFM-induced wind stress to coupled dynamics), and the mature ENSO event, respectively. During the development phase, the subtropical portion of the SST footprint amplifies, peaking during April. This out-of-phase relationship between the SST footprint and the NPO index is consistent with the fact that the NPO is forcing the subtropical SST footprint, as shown in Fig. 4a. During this development, the K_f index amplifies in phase with the winter (0) SST footprint. Note that the CTI is still quite weak during winter (0), and that the K_f lags the NPO. Positive values of the K_f index persist with the SST footprint through the summer (0) transition phase, though NPO variability has ceased. The phase relationships between the K_f index and the NPO and SST footprint indexes in Fig. 5 confirm that it is the zonal wind stress produced through the SFM, rather than that directly produced by the NPO, that is most effective at forcing ENSO.

During the transition phase [summer (0)] and the mature ENSO phase [winter (+1)], the equatorial Pacific

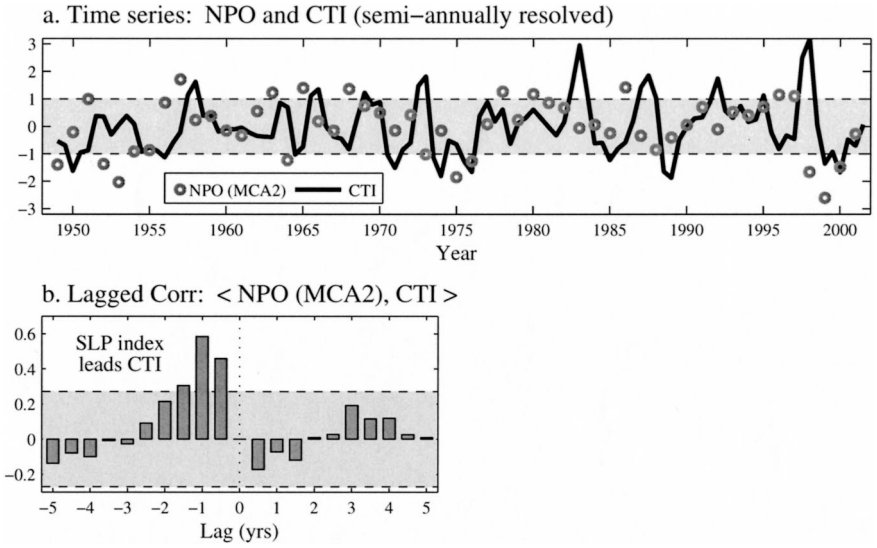

FIG. 6. (a) The winter SLP time series from MCA2 (gray circles) and the semiannually resolved CTI (black line). Both time indices have been standardized. (b) The lagged correlation between the two time series in (a) (bars), plotted with the 95% confidence limits (light shading and dashed lines). Negative lags imply that the SLP index leads the CTI.

Ocean begins to warm with the developing ENSO event, as seen in the CTI evolution. As the equatorial Pacific warms, the positive ''Bjerknes feedback'' (see Zebiak 1985; Battisti 1988; Vimont et al. 2002) acts to amplify K_f, which varies in phase with the CTI through the mature ENSO event. Note that the amplitude of the K_f index during the development and transition periods is one-half to two-thirds of the K_f amplitude at the peak of the mature ENSO phase. The strength and persistence of the SFM-induced wind stress anomalies highlights the potential importance of the SFM in contributing to ENSO development.

4. Implications for ENSO

The strong resemblance between the SST footprint in Fig. 4a and the SST optimal calculated by Penland and Sardeshmukh (1995), combined with the physical interpretation of that SST pattern through the SFM, underscores the potential role of the NPO in producing ENSO variability. This role may be quantified in the observed record by examining the lagged correlation between the (winter only) SLP time series from MCA2 (WIN_NPO) and the semiannually resolved CTI. Because the winter CTI has been linearly removed prior to performing MCA, a null hypothesis of zero correlation is used.[7] The lagged correlation and 95% confidence intervals are plotted in Fig. 6b, along with the actual time series in Fig. 6a. For reference, a lag of -0.5 (-1) yr indicates that the winter (0) SLP index leads the summer (0) [winter ($+1$)] CTI. Figure 6b shows statistically significant correlations when the SLP index *leads* the CTI by up to one and a half years, with a maximum when the SLP index leads the CTI by 1 yr [$r(\tau = -1) = 0.59$], a feature that is confirmed by visual inspection of Fig. 6a. In contrast, there is no indication that the winter midlatitude SLP lags the CTI. Monte Carlo simulations in which the SLP data for MCA2 are randomly scrambled in time prior to performing MCA indicate that the probability of reproducing a 1-yr lead correlation of $r(\tau = -1) = 0.59$ is 0.2% (6 out of 3000 tests). Furthermore, a cross-validated prediction of the winter ($+1$) CTI [by recursively applying the method in MCA2 (Fig. 2) to 52 yr of data, and using the result to predict the winter ($+1$) CTI for the independent year] reproduces a high correlation of $r = 0.46$ between the predicted and actual winter ($+1$) CTI. The significance and asymmetry of the lagged correlation further demonstrates the causality implied by the SFM: midlatitude atmospheric variability is affecting the development of ENSO.

Further inspection of the two time series in Fig. 6a yields some very interesting behavior. It is noted that every El Niño event in the 53-yr record (defined as a winter when the CTI exceeds one standard deviation) is preceded by a positive value of the SLP index. Most notable in the recent record is the extreme El Niño event of 1997–98, which was preceded by 2 yr of NPO-like conditions that exceed one standard deviation. Similarly, with the exception of the 1971 and 1985 events, every La Niña event is preceded by a negative value of the

[7] Due to the linear removal of the winter CTI, the zero correlation null hypothesis used herein is identical to the atmospheric bridge (Alexander 1992; Lau and Nath 1996) null hypothesis used by Vimont et al. (2001) and Vimont et al. (2003).

SLP index. This is especially true of the 1999–2001 period, which experienced persistent mild La Niña conditions preceded by strong negative NPO-like SLP anomalies. Though this relation is expressed statistically by the lagged correlation shown in Fig. 6b, the consistency of the relationship is surprising.

The strong correlation between NPO-like SLP anomalies and tropical SST anomalies 1 yr later implies that ENSO may be in a linearly stable state in nature, and underscores the importance of midlatitude atmospheric variability as a potential leading contributor to the stochastic forcing of ENSO. The relationship between ENSO and its stochastic forcing will depend strongly on the stability of the ENSO mode. If ENSO is in a linearly unstable regime, then ENSO variance is maintained by the ENSO mode itself, and there should be little (nearly zero) correlation between ENSO and its stochastic forcing (the NPO). If the ENSO mode is in a linearly stable state, then ENSO variance is maintained by stochastic forcing. In this latter case, the correlation between ENSO and the NPO will depend on the stability of the ENSO mode and on the relative importance of the NPO to the total stochastic forcing of ENSO. Note that even in a heavily damped system forced only by the NPO, the correlation between ENSO and the NPO should not be unity, due to the dynamics of the ENSO mode. The correlation expressed in Fig. 6 suggests to us that ENSO is somewhere between a heavily damped and nearly neutral regime in nature. In this regime, the Tropics must be ''set up'' for the initiation of an ENSO event (hence, not every strong NPO is followed by an ENSO event) and must also be stochastically forced in such a way as to encourage ENSO growth.

The existence and behavior of the SFM in the observed record has implications for prediction and general understanding of ENSO variability. First, the physical processes inherent to the SFM indicate a potentially important role of the NPO in predicting ENSO. Indeed, the large 1-yr lead correlation exhibited in Fig. 6 is comparable to the performance of state-of-the-art CGCMs. Second, by providing a mechanism by which midlatitude variability can affect ENSO, the SFM may reshape our fundamental understanding of Pacific climate variability. Further study is needed to investigate the physical processes associated with the SFM, as well as its role in affecting the temporal and spatial structure, range, and predictability of Pacific climate variability.

Acknowledgments. Special thanks to E. S. Sarachik at the University of Washington for his suggestions and guidance. Thanks to three anonymous reviewers for their suggestions, to N. Mantua for his comments on the original manuscript, and to numerous individuals at the NOAA Climate Diagnostics Center and at NCAR for conversations about the results. This work was supported by a grant to the Joint Institute for the Study of the Atmosphere and Ocean (JISAO) under NOAA Cooperate Agreement NA17RJ1232.

APPENDIX

Time Index Definitions for Fig. 5

Time indices for Fig. 5 are calculated in the following manner.

a. NPO

A 3-month running mean is applied to the monthly resolved SLP data. The data are standardized, and a series of lagged regression maps are generated by regressing the SLP data for each calendar month onto the annually resolved SLP index from MCA2. Finally, each regression map is projected onto the spatial SLP pattern from MCA2, resulting in a monthly resolved index plotted in Fig. 5. This index represents the (relative) amplitude of the NPO for a given month relative to the winter (0) WIN_NPO index.

b. Subtropical SST footprint

The SST footprint index is calculated similarly to the NPO index, except that nonstandardized SST data are used, and the projection is taken between the monthly lagged regression maps and the winter (0) regression map of SST onto the WIN_NPO index, over the region 6°–20°N, 150°E–110°W. The resulting index represents the relative amplitude of subtropical SST anomalies for a given month relative to the winter (0) WIN_NPO index. For reference, the maximum projection (in April) corresponds to SST anomalies of about 0.2°–0.3°C in the subtropical portion of the SST footprint (see Fig. 4a).

c. K_f index

The K_f index is calculated similarly to the NPO index, except regression maps are generated using the zonal wind stress data from 120°E to 150°W. Each regression map is then projected onto the meridional Kelvin wave structure [see Battisti (1988, appendix A) for details]: $K_f(x, \lambda) = \int_{-30^\circ}^{30^\circ} \tau_x(x, y, \lambda)\psi_0(y)\, dy$, where $\psi_0(y)$ is the meridional equatorial Kelvin wave structure, and $\tau_x(x, y, \lambda)$ is the zonal wind stress map for a given lag λ. Results are generally insensitive to realistic values for the equivalent depth of the first baroclinic mode, used to calculate $\psi_0(y)$ [see also Vimont et al. (2003, section 5)]. The K_f index is the zonal mean of $K_f(x, \lambda)$ and indicates the effectiveness of a given wind stress map at forcing oceanic equatorial Kelvin signals. Positive values indicate a forcing of downwelling Kelvin signals, which will tend to warm the equatorial Pacific.

d. CTI

The CTI index in Fig. 5 is generated by applying a 3-month running mean to the monthly resolved CTI and

regressing that data for each calendar month onto the winter (0) WIN_NPO index. Units indicate the typical amplitude of the CTI at a given lag from the winter (0) WIN_NPO index. For reference, the standard deviation of the winter (0) CTI is 0.9°C.

REFERENCES

Alexander, M. A., 1992: Midlatitude atmosphere–ocean interaction during El Niño. Part II: The Northern Hemisphere atmosphere. *J. Climate,* **5,** 959–972.

Barnett, T. P., D. W. Pierce, M. Latif, D. Dommenget, and R. Saravanan, 1999: Interdecadal interactions between the tropics and midlatitudes in the Pacific basin. *Geophys. Res. Lett.,* **26** (5), 615–618.

Battisti, D. S., 1988: Dynamics and thermodynamics of a warming event in a coupled tropical atmosphere–ocean model. *J. Atmos. Sci.,* **45,** 2889–2919.

Bretherton, C. S., C. Smith, and J. M. Wallace, 1992: An intercomparison of methods for finding coupled patterns in climate data. *J. Climate,* **5,** 541–560.

——, M. Widmann, V. P. Dymnikov, J. M. Wallace, and I. Bladé, 1999: The effective number of spatial degrees of freedom of a time-varying field. *J. Climate,* **12,** 1990–2009.

Chiang, J. C. H., S. Zebiak, and M. A. Cane, 2001: Relative roles of elevated heating and surface temperature gradients in driving anomalous surface winds over tropical oceans. *J. Atmos. Sci.,* **53,** 1371–1394.

Czaja, A., P. van der Vaart, and J. Marshall, 2002: A diagnostic study of the role of remote forcing in tropical Atlantic variability. *J. Climate,* **15,** 2310–2324.

Deser, C., and M. S. Timlin, 1997: Atmosphere–ocean interaction on weekly timescales in the North Atlantic and Pacific. *J. Climate,* **10,** 393–408.

Gill, A. E., 1980: Some simple solutions for heat-induced tropical circulation. *Quart. J. Roy. Meteor. Soc.,* **106,** 447–462.

Harrison, D. E., and N. K. Larkin, 1998: El Niño–Southern Oscillation sea surface temperature and wind anomalies, 1946–1993. *Rev. Geophys.,* **36,** 353–400.

Kalnay, E., and Coauthors, 1996: The NCEP/NCAR 40-year reanalysis project. *Bull. Amer. Meteor. Soc.,* **77,** 437–471.

Larkin, N. K., and D. E. Harrison, 2001: Tropical Pacific ENSO cold events, 1946–95: SST, SLP, and surface wind composite anomalies. *J. Climate,* **14,** 3904–3931.

Lau, N.-C., and M. J. Nath, 1996: The role of the ''atmospheric bridge'' in linking tropical Pacific ENSO events to extratropical SST anomalies. *J. Climate,* **9,** 2036–2057.

Liebmann, B., and C. A. Smith, 1996: Description of a complete (interpolated) outgoing longwave radiation dataset. *Bull. Amer. Meteor. Soc.,* **77,** 1275–1277.

Penland, C., and P. D. Sardeshmukh, 1995: The optimal growth of tropical sea surface temperature anomalies. *J. Climate,* **8,** 1999–2024.

Pierce, D. W., T. P. Barnett, and M. Latif, 2000: Connections between the Pacific Ocean Tropics and midlatitudes on decadal timescales. *J. Climate,* **13,** 1173–1194.

Rogers, J. C., 1981: The North Pacific Oscillation. *J. Climatol.,* **1,** 39–57.

Vimont, D. J., 2002: The seasonal footprinting mechanism in the CSIRO coupled general circulation models and in observations. Ph.D. dissertation, University of Washington, 91 pp.

——, D. S. Battisti, and A. C. Hirst, 2001: Footprinting: A seasonal connection between the tropics and mid-latitudes. *Geophys. Res. Lett.,* **28** (20), 3923–3926.

——, ——, and ——, 2002: Pacific interannual and interdecadal equatorial variability in a 1000-yr simulation of the CSIRO coupled general circulation model. *J. Climate,* **15,** 160–178.

——, ——, and ——, 2003: The seasonal footprinting mechanism in the CSIRO general circulation models. *J. Climate,* **16,** 2653–2667.

Walker, G. T., and E. W. Bliss, 1932: World weather V. *Mem. Roy. Meteor. Soc.,* **4,** 53–84.

Zebiak, S. E., 1985: Tropical atmosphere–ocean interaction and the El Niño/Southern Oscillation phenomenon. Ph.D. thesis, Massachusetts Institute of Technology, 261 pp.